doi:10.1093/plcell/koab175

THE PLANT CELL

THE PLANT CELL 2021: 33: 3120–3133

Research Article

AUXIN RESPONSE FACTORS 6 and 17 control the flag leaf angle in rice by regulating secondary cell wall biosynthesis of lamina joints

Guoqiang Huang [1], Heng Hu [1], Allison van de Meene [2], Jiao Zhang [1], Le Dong [1], Shuai Zheng [3], Fengli Zhang [1], Natalie S. Betts [4], Wanqi Liang [1], Malcolm J. Bennett [5], Staffan Persson [1,2,3,6] and Dabing Zhang [1,4,*,†]

1 Joint International Research Laboratory of Metabolic & Developmental Sciences, State Key Laboratory of Hybrid Rice, SJTU-University of Adelaide Joint Centre for Agriculture and Health, School of Life Sciences and Biotechnology, Shanghai Jiao Tong University, Shanghai, China
2 School of Biosciences, University of Melbourne, Parkville VIC 3010, Melbourne, Australia
3 Department of Plant & Environmental Sciences, University of Copenhagen, 1871, Frederiksberg C, Denmark
4 School of Agriculture, Food and Wine, University of Adelaide, Waite Campus, Urrbrae, South Australia
5 Future Food Beacon and School of Biosciences, University of Nottingham, LE12 5RD, UK
6 Copenhagen Plant Science Center, University of Copenhagen, 1871, Frederiksberg C, Denmark

*Author for correspondence: zhangdb@sjtu.edu.cn
†Senior author.

G.H., D.Z., S.P., and M.J.B. designed the research; G.H., H.H., A.v.d.M., J.Z., L.D., S.Z., and F.Z. performed the research; G.H., H.H., J.Z., and L.D. contributed the analytical tools and analyzed the data; and G.H., D.Z., S.P., W.L., N.S.B., and M.J.B. wrote this manuscript. The final manuscript was approved by all the authors.

The author(s) responsible for distribution of materials integral to the findings presented in this article in accordance with the policy described in the Instructions for Authors (https://academic.oup.com/plcell) is: Dabing Zhang (zhangdb@sjtu.edu.cn).

Abstract

Flag leaf angle impacts the photosynthetic capacity of densely grown plants and is thus an important agronomic breeding trait for crop architecture and yield. The hormone auxin plays a key role in regulating this trait, yet the underlying molecular and cellular mechanisms remain unclear. Here, we report that two rice (*Oryza sativa*) auxin response factors (ARFs), OsARF6 and OsARF17, which are highly expressed in lamina joint tissues, control flag leaf angle in response to auxin. Loss-of-function double *osarf6 osarf17* mutants displayed reduced secondary cell wall levels of lamina joint sclerenchymatous cells (Scs), resulting in an exaggerated flag leaf angle and decreased grain yield under dense planting conditions. Mechanical measurements indicated that the mutant lamina joint tissues were too weak to support the weight of the flag leaf blade, resembling the phenotype of the rice *increased leaf angle1* (*ila1*) mutant. We demonstrate that OsARF6 and OsARF17 directly bind to the *ILA1* promoter independently and synergistically to activate its expression. In addition, auxin-induced *ILA1* expression was dependent on OsARF6 and OsARF17. Collectively, our study reveals a mechanism that integrates auxin signaling with the secondary cell wall composition to determine flag leaf angle, providing breeding targets in rice, and potentially other cereals, for this key trait.

Received March 19, 2021. Accepted June 28, 2021. Advance access publication July 10, 2021

IN A NUTSHELL

Background: The flag leaf is the top leaf on a rice stem, closest to the grain-producing panicle. Flag leaves have a major role in providing energy to the developing grain, and any impact on photosynthesis in the flag leaf can have a dramatic effect on grain productivity. In a rice field, overall yield per area depends on maximizing plant density, so crop lines with erect flag leaves are preferred; these plants can be planted more closely together without compromising grain yield per plant. The angle of the flag leaf to the main stem is primarily determined by the shape and structure of the lamina joint, which connects the flag leaf to the stem. The cellular organization in the lamina joint maintains flag leaf erectness, so appropriate cell elongation on both sides of the joint, the development of mechanical tissues, and cell wall composition, all impact flag leaf angle.

Question: We wanted to know whether and how auxin, a plant hormone known to be involved in a range of developmental pathways, may modulate flag leaf angle in rice. We investigated this mainly by looking at the expression of auxin-responsive factors, OsARF6 and OsARF17.

Findings: We found that both *OsARF6* and *OsARF17* genes were highly expressed in flag leaf lamina joints. Knockout mutants that lacked functional OsARF6 and OsARF17 exhibited larger flag leaf angles, and were found to have abnormal secondary cell walls. Yield was decreased in the knockout mutants in densely planted conditions. We identified a third gene, ILA1, which directs secondary cell wall biosynthesis in rice, was directly activated by OcARF6 and OsARF17 independently and synergistically, revealing a pathway that controls flag leaf angle.

Next steps: Fine-tuning this auxin signaling pathway can provide better control of flag leaf angles in elite rice cultivars, allowing for greater planting densities and therefore higher yield. Understanding this new pathway provides promising new targets for rice breeders and further research in the future.

Introduction

Flag leaf angle refers to the inclination between the flag leaf blade and vertical culm in grass species (Moldenhauer et al., 2003; Zhou et al., 2017). The flag leaf is the uppermost leaf closest to the panicle, featuring the highest photosynthetic capacity, and plays a major role in determining grain productivity (Chen et al., 2007; Dong et al., 2018). As overall yield depends on maximizing plant density, crop lines with erect flag leaves that can tolerate a denser planting rate are preferred (Jiao et al., 2010; Zhou et al., 2017; Tian et al., 2019). The flag leaf angle is primarily determined by the shape and structure of the lamina joint, which connects the flag leaf blade and culm (Zhou et al., 2017). The cellular organization in the lamina joint maintains flag leaf erectness, so appropriate cell elongation of abaxial and adaxial sides, the development of mechanical tissues, and cell wall composition all impact the flag leaf angle (Ning et al., 2011; Zhao et al., 2013).

Genetic studies have identified several genes and signals which impact flag leaf angle in rice, including *Increased Leaf Angle1* (*ILA1*), a Raf-like mitogen-activated protein kinase kinase kinase (MAPKKK) of group C with serine/threonine kinase activity. In comparison with wild-type (WT) plants, *ila1* loss-of-function mutant lines exhibit a larger flag leaf angle due to the reduced mechanical strength of lamina joints (Ning et al., 2011). Further research identified ILA1-interacting protein 4 (IIP4) that, after phosphorylation by ILA1, translocated from the nucleus to the cytoplasm to promote the secondary cell wall biosynthesis (Zhang et al., 2018).

Phytohormones are associated with the control of flag leaf angle in rice. Brassinosteroids (BRs) promote cell elongation and propagation at the adaxial side of the lamina joint (Cao and Chen, 1995; Bai et al., 2007; Sun et al., 2015; Tian et al., 2019), and flag leaf angle is positively correlated with BR levels at the lamina joint (Yamamuro et al., 2000; Hong et al., 2002, 2003; Sakamoto et al., 2006; Li et al., 2009, 2013). Gibberellin modulates leaf angles by promoting cell expansion and cell proliferation of parenchymal cells especially on the abaxial side of lamina joints (Ueguchi-Tanaka et al., 2000; Shimada et al., 2006; Tong et al., 2014; Chen et al., 2020). Auxin promotes the elongation of parenchyma cells to regulate the leaf angle (Zhao et al., 2013; Zhang et al., 2015). Reduction in free auxin content in lamina joint tissues results in increased flag leaf angle (Zhang et al., 2009, 2015; Du et al., 2012; Zhao et al., 2013). Despite the importance of auxin in flag leaf angle regulation, the molecular and cellular mechanisms underpinning its role remain largely unclear.

Here, we uncover an auxin-mediated regulatory network determining flag leaf angle by modulating the secondary cell wall biosynthesis in lamina joint tissues. We show that two paralogous auxin response factors (ARFs), OsARF6 and OsARF17 (Shen et al., 2010), regulate flag leaf angle in rice in response to auxin. Loss-of-function mutants of *OsARF6* and *OsARF17* displayed larger flag leaf angles due to the reduced mechanical strength of the lamina joints caused by decreased the secondary cell wall deposition; this, in turn, led to reduced grain yield in dense planting conditions. Furthermore, we demonstrate that *OsARF6* and *OsARF17* are

epistatic to *ILA1* and directly regulate the expression of *ILA1* to control flag leaf angle.

Results

Mutants lacking OsARF6 exhibit large flag leaf angles

Auxin regulates flag leaf angle in rice and reduced levels of free auxin (indole-3-acetic acid) in lamina joints result in larger leaf angles (Zhang et al., 2009; Du et al., 2012; Zhao et al., 2013). We further explored this phenomenon by treating WT rice flag leaf joints with 1-naphthaleneacetic acid (NAA, a synthetic auxin) and found a reduction in flag leaf angle (Figure 1, A to C). To unravel the mechanistic basis by which auxin influences flag leaf angle, we examined T-DNA insertion mutants that disrupt *ARF* genes, which encode central components of the auxin signaling machinery (Wu et al., 2003; Zhang et al., 2006, 2014). Intriguingly, we observed an increased flag leaf angle (Figure 1, D to F) in a mutant line with T-DNA inserted in the 5′-untranslated region of *OsARF6*, hence named *osarf6* (RMD_04Z11MS49; Supplemental Figure S1A). Unlike in WT plants, *OsARF6* transcripts were not detected in *osarf6* flag leaf lamina joints (Supplemental Figure S1B), indicating that it is a transcriptional null mutant. To confirm transcription of *OsARF6* in flag leaf lamina joints, we constructed *ProOsARF6:GUS* transgenic reporter lines for histochemical analysis. Strong reporter signals were detected in lamina joints of reporter lines, revealing that *OsARF6* was highly expressed in the flag leaf lamina joints from an early stage, with expression declining at later stages (Figure 1, G to I). We detected no differences in GUS signals at the abaxial versus adaxial regions of the flag leaf lamina joints in these transgenic plants (Supplemental Figure S2, A and C). To conclude, *OsARF6* is expressed in the lamina joints of flag leaf and is important for flag leaf angle maintenance.

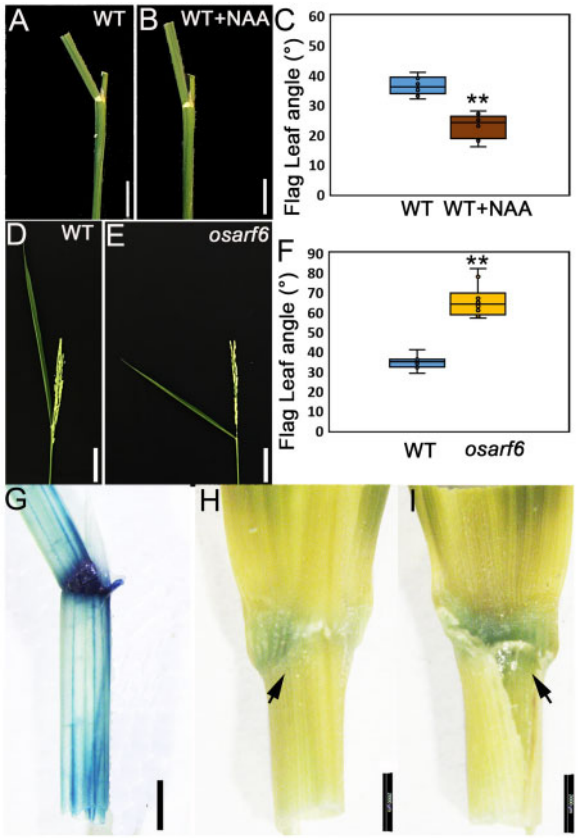

Figure 1 Auxin plays negative roles in regulating flag leaf angle. A, B, WT flag leaf without (A) and with (B) 0.1-μM NAA treatment. Bars, 1 cm. (C) Flag leaf angle analysis of the WT in response to NAA treatment. Boxplots show the distribution of flag leaf angles in the WT without and with NAA treatment. The horizontal bar within box represents median. The top and bottom of the box represent the 0.75 and 0.25 percentiles, respectively. The upper and lower whiskers extend to 1.5 times the interquartile range, with outliers shown as black dots. Two asterisks indicate significant differences (Student's *t* test, $P < 0.01$). D, E, WT (D) and *osarf6* (E) flag leaves. Bars, 5 cm. F, Flag leaf angle analysis of WT and *osarf6* plants. Boxplots show the distribution of flag leaf angles in the WT and *osarf6*. The horizontal bar within box represents median. The top and bottom of the box represent the 0.75 and 0.25 percentiles, respectively. The upper and lower whiskers extend to 1.5 times the interquartile range, with outliers shown as black dots. Two asterisks indicate significant differences (Student's *t* test, $P < 0.01$). G, GUS staining of the flag leaf lamina joints of *ProARF6:GUS* transgenic plants at 65 days after planting. Bar, 5 mm. H, I, GUS staining for abaxial (H) and adaxial (I) regions of the flag leaf lamina joints of *proARF6::GUS* transgenic plants at 80 days after planting. Bars, 200 μm.

Both OsARF6 and OsARF17 regulate flag leaf angles

A yeast-two-hybrid (Y2H) screen revealed that OsARF6 can interact with OsARF17 (Figure 2A), which is the closest homolog of OsARF6 (Shen et al., 2010). The in vivo interaction of these two proteins was confirmed using co-immunoprecipitation (Co-IP) and bimolecular fluorescence complementation (BiFC) assays in *Nicotiana benthamiana* leaves (Figure 2, B–K). Transgenic *ProOsARF17:GUS* reporter lines confirmed that *OsARF17* was also highly expressed in both the abaxial and adaxial regions of lamina joints of flag leaves (Figure 2, L–N; Supplemental Figure S2, A and C), similar to that of *OsARF6*. These data indicate that OsARF17 might work together with OsARF6 to regulate flag leaf angle.

Analysis of a loss-of-function *OsARF17* mutant (Supplemental Figure S1; Li et al., 2020) revealed that *osarf17* plants exhibited WT-like flag leaf angles (Figure 2, O and P), implying that OsARF17 may be less important than OsARF6 in maintaining the flag leaf angle. To examine how OsARF6 and OsARF17 contribute to this function, we crossed the two single mutant lines to generate the double *osarf6 osarf17* mutant (hereafter named *dm* for simplicity). Phenotypic characterization revealed an enhanced phenotype (i.e. an increase in flag leaf angle) in the *dm* over the *osarf6* single mutant (Figure 2, O and P), implying that mutation in *OsARF17* enhances the flag leaf angle defects of *osarf6*.

As we only had one T-DNA line for each of the two *ARF* genes, we created further *osarf6*, *osarf17*, and *dm* mutant lines using CRISPR/Cas9 technology. An A or T insertion in

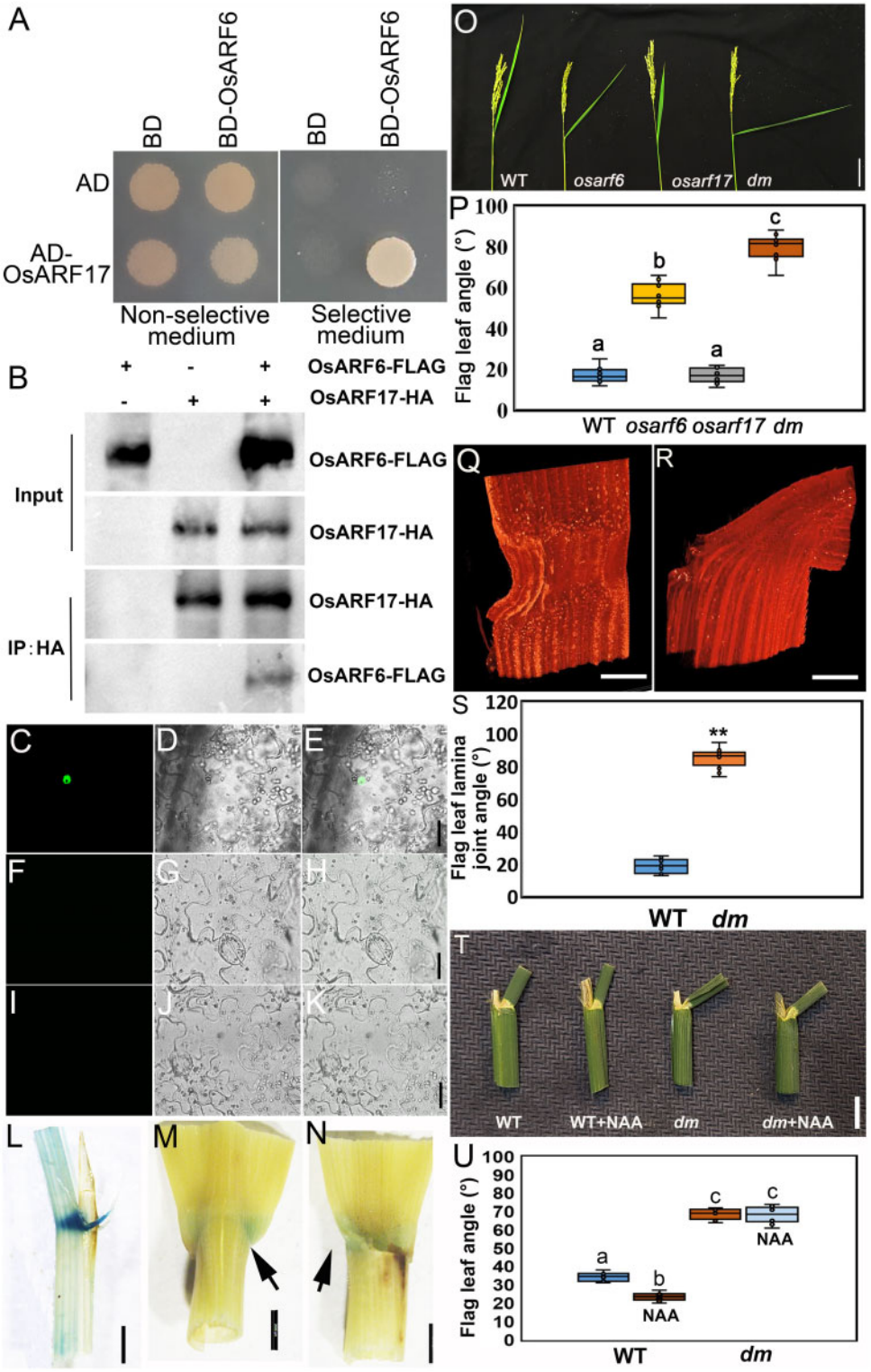

Figure 2 Both OsARF6 and OsARF17 regulate flag leaf angle. A, Y2H assays to detect the interaction between OsARF6 and OsARF17. B, Co-IP assays to detect the interaction between OsARF6-FLAG and OsARF17-HA proteins transiently expressed in *N. benthamiana* leaves. C–E, BiFC assays to detect the interaction between OsARF6-CeYFP and NeYFP-OsARF17 in epidermal cells of leaves of 18-day-old *N. benthamiana* plants. Fluorescence field (C); bright field (D); merged image (E). Bars, 20 μm. F–H, BiFC assays to detect the interaction between OsARF6-CeYFP and NeYFP in epidermal cells of leaves of 18-day-old *N. benthamiana* plants. Fluorescence field (F); bright field (G); merged image (H). Bars, 20 μm. I–K, BiFC assays to detect the interaction between CeYFP and NeYFP-OsARF17 in epidermal cells of leaves of 18-day-old *N. benthamiana* plants. Fluorescence field (I); bright field (J); merged image (K). Bars, 20 μm. (L) GUS staining of the flag leaf lamina joints of *ProARF17:GUS* transgenic plants at 65 days after planting. Bar, 5 mm. M, N, GUS staining for abaxial (E) and adaxial (F) regions of the flag leaf lamina joints of *ProARF17:GUS* transgenic plants at 80 days after planting. Bars, 200 μm. O, WT, *osarf6*, *osarf17*, and *dm* flag leaves at 90 days after planting. Bar, 5 cm. P, Flag leaf angle analysis of WT, *osarf6*, *osarf17*, and *dm* plants. Boxplots show the

the second exon of both genes created frameshifts that successfully disrupted the genes (Supplemental Figure S3A). Consistent with the observed phenotypes of the T-DNA insertion mutants, we observed increased flag leaf angles in *osarf6* (Supplemental Figure S3, B and C), and a stronger flag leaf angle phenotype in the four independent *dm* CRISPR/Cas9 lines (Supplemental Figure S3, D and E), confirming that OsARF6 and OsARF17 regulate lamina joint development of the flag leaf.

The flag leaf angle is mainly determined by properties of the lamina joint tissues, which connect the base of the leaf blade to the culm (Zhou et al., 2017). To analyze the morphology of flag leaf lamina joints, we used X-ray microcomputed tomography (microCT) to nondestructively 3D image WT and *dm* tissues (Mairhofer et al., 2013). MicroCT imaging revealed that *dm* plants developed an almost rectangular lamina joint compared to the erect lamina joint of WT plants (Figure 2, Q–S; Supplemental Movies S1 and S2). Apart from the flag leaf angle, no obvious phenotypic differences were observed in plant height, other leaf angles, and tiller angles of WT, *osarf6*, *osarf17*, and *dm* plants at the tillering stage (Supplemental Figure S4, A to E), indicating that flag leaf angle modulation is likely to be the main regulatory function of OsARF6 and OsARF17 proteins.

Whereas *OsARF6* and *OsARF17* exhibited the highest expression in the lamina joints of flag leaves, other *ARF*s, such as *OsARF6*, *OsARF12*, *OsARF17*, and *OsARF25*, showed less expression in this tissue and were instead expressed in other tissues, such as lamina joints of leaves and roots (Supplemental Figure S5, A and B). To better understand any compensatory relationships between *OsARF6* and *OsARF17*, we undertook reverse transcription quantitative polymerase chain reaction (RT-qPCR) analyses of the expression levels of the two genes in the different genotypes. Here, we did not detect any increase in *OsARF6* transcript in *osarf17* as compared to the WT (Supplemental Figure S5C), indicating a less prominent role of OsARF17 in flag leaf lamina joint development.

OsARF6 and OsARF17 are presumably two central components of the auxin signaling pathway (Shen et al., 2010). To test whether these ARFs responded to auxin to modulate flag leaf angle, we applied NAA to WT and *dm* flag leaf lamina joints. The *dm* plants responded less strongly than the WT to exogenous NAA (Figure 2, T and U), indicating that auxin regulates the flag leaf angle through OsARF6 and OsARF17. It is worth noting that the overexpression of *OsARF6* or *OsARF17* did not lead to significant differences in comparison to the flag leaf angle of the WT (Supplemental Figure S5, D–G). We speculate that the already narrow angle in the WT used in our study, i.e. ZH11, may not be further decreased by the action of ARFs.

OsARF6 and OsARF17 regulate the secondary cell wall biosynthesis and the mechanical strength of the flag leaf lamina joints

The flag leaf angle is determined by the mechanical properties of tissues that make up the lamina joints (Zhou et al., 2017; Wang et al., 2020). To pinpoint the differences between tissues in WT and *dm* lamina joints, we initially examined their anatomical structures. High-resolution microCT imaging revealed a reduction in the secondary cell wall thickness of sclerenchymatous cell (Sc) in *dm* compared with WT lines (Figure 3, A–G; Supplemental Movies S3 and S4), indicating that the mechanical properties were altered in *dm* lamina joints. The Sc tissue is largely responsible for providing sufficient mechanical strength to maintain flag leaf erectness (Ning et al., 2011), so we hypothesized that the increased flag leaf angle of *dm* plants resulted from the reduced mechanical strength due to defective Sc formation. Our analysis of the minimum force required to break the lamina joints revealed that *dm* flag leaves could be broken off with only ~25% of the minimum force required to break WT lamina joints (Figure 3H).

Sc in the lamina joint feature thickened secondary cell walls mainly comprising cellulose, hemicellulose, and lignin (Kang et al., 2019). Lignin staining by phloroglucinol–HCl revealed reduced lignin deposition in the lamina joints of *dm* flag leaves, but not stems, compared to the WT (Figure 4, A–H; Supplemental Figure S6, A–F). Large differences in the lignin content were observed in abaxial Sc in WT and *dm* lamina joints (Figure 4, A–D), while Sc in adaxial tissues was not lignin-rich in either WT or *dm* lamina joints (Figure 4, E–H). Cellulose labeling showed brighter fluorescence in the WT compared with *dm* lamina joints, on both abaxial and adaxial sides (Figure 4, I–P; Supplemental Figure S6G), indicating that cellulose biosynthesis was disrupted when *OsARF6* and *OsARF17* were mutated. In contrast, cellulose content in

distribution of flag leaf angles in WT, *osarf6*, *osarf17*, and *dm*. The horizontal bar within box represents median. The top and bottom of the box represent the 0.75 and 0.25 percentiles, respectively. The upper and lower whiskers extend to 1.5 times the interquartile range, with outliers shown as black dots. Different letters indicate significant differences (Student's *t* test, $P < 0.01$). Q, R, MicroCT imaging of flag leaf lamina joints of WT and *dm* at 90 days after planting. Bar, 2 mm. S, Analysis of flag-leaf lamina-joint angles of WT and *dm* plants. Boxplots show the distribution of the lamina joint angles of flag leaves in the WT and *dm*. The horizontal bar within box represents median. The top and bottom of the box represent the 0.75 and 0.25 percentiles, respectively. The upper and lower whiskers extend to 1.5 times the interquartile range, with outliers shown as black dots. Two asterisks indicate significant differences (Student's *t* test, $P < 0.01$). T, WT and *dm* flag leaves with/without NAA treatment. Bar, 1 cm. U, Flag leaf angle analysis of WT and *dm* plants with/without NAA treatment for 14 days. Boxplots show the distribution of flag leaf angles in the WT and *dm* with/without NAA treatment. The horizontal bar within box represents the median. The top and bottom of the box represent the 0.75 and 0.25 percentiles, respectively. The upper and lower whiskers extend to 1.5 times the interquartile range, with outliers shown as black dots. Different letters indicate significant differences (Student's *t* test, $P < 0.01$).

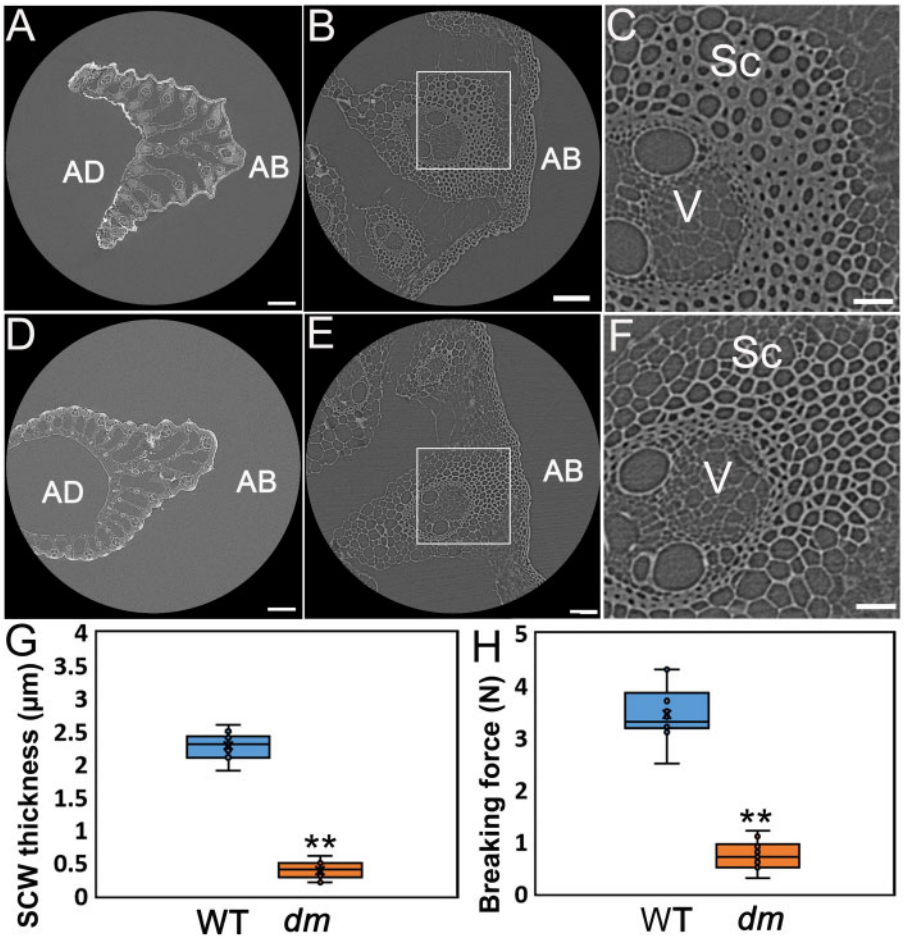

Figure 3 OsARF6 and OsARF17 determine flag leaf angle by affecting the secondary cell wall synthesis. A–F, CT sections of the WT ([A] to [C]) and *dm* ([D] to [F]) flag leaf lamina joints. A, D, CT sections of whole joint. AB, abaxial; AD, adaxial; bar, 500 μm. ([B], [C], [E], and [F]) Closer examination of abaxial sections in WT ([B], boxed region expanded in [C]) and *dm* ([E], boxed region expanded in [F]). Bars ([B] and [E]), 100 μm, Bars ([C] and [F]), 20 μm. V, vascular bundle. G, The thickness of secondary cell wall (SCW) of Sc in WT and *dm* flag leaf lamina joints. Boxplots show the distribution of SCW thickness in the WT and *dm*. The horizontal bar within box represents the median. The top and bottom of the box represent the 0.75 and 0.25 percentiles, respectively. The upper and lower whiskers extend to 1.5 times the interquartile range, with outliers shown as black dots. Two asterisks indicate significant differences (Student's *t* test, $P < 0.01$). H, The minimum force required to break WT and *dm* lamina joints of the WT and *dm*. Boxplots show the distribution of minimum breaking force to breaking the lamina joints in the WT and *dm*. The horizontal bar within box represents median. The top and bottom of the box represent the 0.75 and 0.25 percentiles, respectively. The upper and lower whiskers extend to 1.5 times the interquartile range, with outliers shown as black dots. Two asterisks indicate significant differences (Student's *t* test, $P < 0.01$).

stems was unaffected by the *dm* mutation (Supplemental Figure S6H). These results demonstrate that OsARF6 and OsARF17 regulate the secondary cell wall biosynthesis in Sc of flag leaf lamina joints, affecting the physical strength of the lamina joints to support the weight of the flag leaf blade.

One intriguing question is whether a differential weight gain of flag leaf blades in the WT and *dm* would be the reason for the larger flag leaf angle in *dm* plants. To address this point directly, we measured the weight of the flag leaf blade in WT and *dm* plants from 60 to 90 days after planting. There was a steep increase in the weight of the flag leaf blade from 70 to 75 days in both WT and *dm* plants (Supplemental Figure S7, A–C). Moreover, there was also no significant difference in flag leaf weight in the two lines from 70 to 90 days (Supplemental Figure S7C). Correspondingly, *dm* plants exhibited a dramatic increase in flag leaf angle at 75 days after planting, at the time when flag leaf weight increased significantly (Supplemental Figure S7D). These results indicate that the increased flag leaf angle in *dm* plants was due to the reduced mechanical strength of the lamina joint that was unable to support the weight of the mature flag leaf blade, which was unaffected by mutations.

OsARF6 and OsARF17 directly co-regulate *ILA1* expression

As ARF activators, OsARF6 and OsARF17 function by activating the expression of downstream genes by binding to specific promoter elements (i.e. Aux RE: TGTCTC; Aux RE-L: TGTCNN; Shen et al., 2010; Freire-Rios et al., 2020). We set out to determine what downstream components OsARF6 and OsARF17 may regulate. One possible target would be

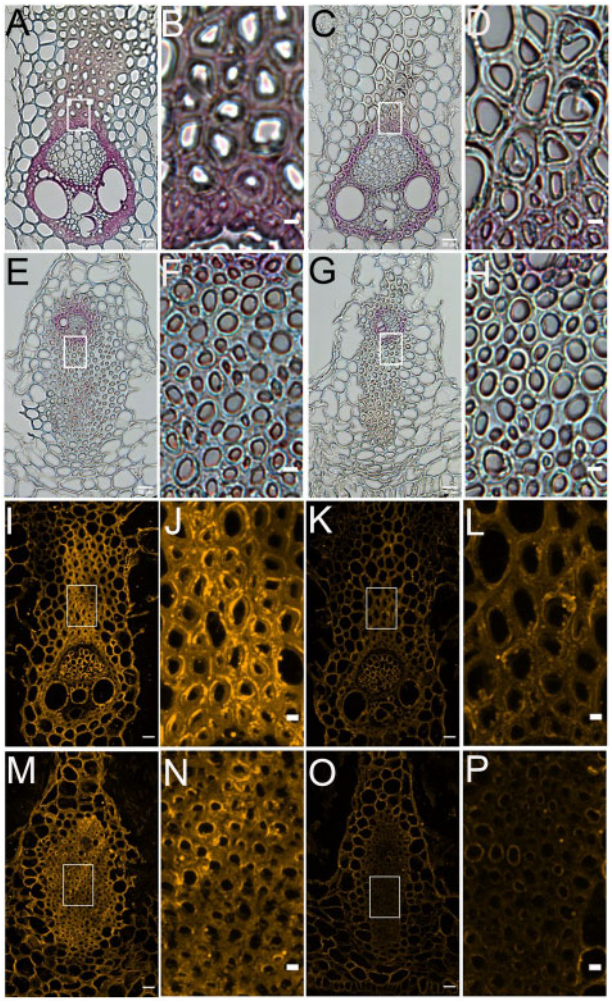

Figure 4 Lignin and cellulose contents are reduced in *dm* lamina joints. A–H, Lignin staining by phloroglucinol–HCl. Red/pink lignin staining in cells surrounding the vascular bundle and Sc on abaxial (A–D) and adaxial (E–H) sides of WT (A, B, E, and F) and *dm* (C, D, G, and H) lamina joints. B, D, F, and H, show higher magnification images of sclerenchymatous regions boxed in (A), (C), (E), and (G), respectively. Bars (A, C, E, and G) 20 μm, (B, D, F, and H) 5 μm. I–P, Cellulose labeling in cells surrounding the vascular bundle and Sc on abaxial (I–L) and adaxial (M–P) sides of WT (I, J, M, and N) and *dm* (K, L, O, and P) lamina joints. J, L, N, and P, show higher magnification images of sclerenchymatous regions boxed in (I), (K), (M), and (O), respectively. Bars (I, K, M, and O) 20 μm, (J, L, N, and P) 5 μm.

ILA1, as mutations in this gene lead to a large flag leaf angle and altered cell wall composition in the lamina joints (Ning et al., 2011; Zhang et al., 2018). Consistent with reported results, lignin and cellulose levels were reduced in the flag leaf lamina joint, but not in the stem, of *ila1* plants (Supplemental Figure S8; Zhang et al., 2018), resembling the *dm* phenotype (Supplemental Figure S6). Furthermore, high-resolution microCT imaging revealed that the secondary cell wall thickness of Sc was thinner in *dm* lamina joints as compared to the WT (Supplemental Figure S9), indicating that *ILA1* regulates flag leaf angles in the same pathway as *OsARF6* and *OsARF17*. In addition, both types of cis-acting elements (17 Aux RE-L and 1 Aux RE motifs) were found in the 2,445-bp region upstream of the *ILA1* start codon (Figure 5A), implying that it is likely to be activated by ARFs.

To verify the interactions between *ILA1* and OsARF6/17, we first conducted a yeast one-hybrid (Y1H) assay. Yeast expressing *OsARF6* or *OsARF17* cDNAs that were transformed with the *ILA1* promoter constructs grew on the selective medium (Figure 5B), demonstrating that OsARF6 and OsARF17 can both directly bind to the promoter of *ILA1*. To confirm the interaction between OsARF6, OsARF17, and the *ILA1* promoter, we undertook dual-luciferase (LUC) assays by transiently co-expressing *ProILA1:LUC* with *Pro35S:OsARF6* and/or *Pro35S:OsARF17* in *N. benthamiana* leaves. A significant increase of LUC activity was detected in the presence of OsARF6 or OsARF17 compared with the empty vector, which was further increased when OsARF6 and OsARF17 were co-expressed (Supplemental Figure S10A), indicating that OsARF6 and OsARF17 can act synergistically to activate *ILA1* transcription.

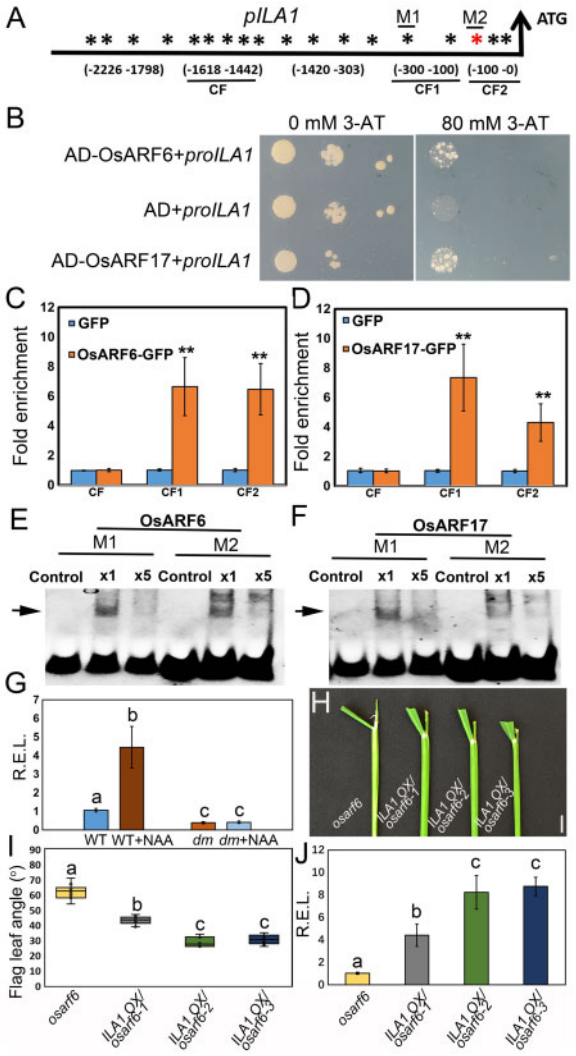

Figure 5 OsARF6 and OsARF17 directly co-regulate *ILA1* expression. A, Diagram of the *ILA1* promoter region. Red asterisks: Auxin Response Element (Aux RE; TGTCTC); black asterisks: Auxin Response Element-like (Aux RE-L; TGTCNN). Upstream nucleotide numbering is relative to the start codon (A is +1). B, Y1H assays to detect interaction between OsARF6/17 and promotor of *ILA1*. C, D, ChIP–qPCR assays to detect interaction in flag leaf lamina joints between OsARF6/17 and CF1/2 indicted in (A). CF1 fragment contains three Aux RE-Ls; CF2 comprises one Aux RE and two Aux RE-Ls. Results are given as mean ± SE calculated with three biological replicates. Different characters indicate significant differences (Student's *t* test, $P < 0.01$). E, F, EMSAs to detect interaction between OsARF6/17 and M1/2 (M1, Aux RE-L motif of CF1; M2, Aux RE motif of CF2) probes. G, Relative expression level (R.E.L.) of *ILA1* in WT and *dm* lamina joints with/without NAA treatment for 2 h. Results are given as mean ± SE calculated with three biological replicates. Different characters indicate significant differences (Student's *t* test, $P < 0.01$). H, Phenotypes of *osarf6* and overexpressing *ILA1* in *osarf6* lines (*ILA1 OX*/*osarf6*). Bar, 1 cm. I, Flag leaf angle analysis of *osarf6*, and *ILA1* overexpression in *osarf6* lines. Boxplots show the distribution of minimum breaking force to breaking the lamina joints in *osarf6*, and *ILA1* overexpression in *osarf6* lines. The horizontal bar within box represents the median. The top and bottom of the box represent the 0.75 and 0.25 percentiles, respectively. The upper and lower whiskers extend to 1.5 times the interquartile range, with outliers shown as black dots. Different letters indicate significant differences (Student's *t* test, $P < 0.01$). J, Relative expression levels (R.E.L.) of *ILA1* in *osarf6* and *ILA1* overexpression *OX*/*osarf6* lines. Results are given as mean ± SE calculated from three biological replicates. Different letters indicate significant differences (Student's *t* test, $P < 0.01$).

To functionally dissect *ILA1* promoter activity, we constructed a series of truncated *ILA1* promoter fragments fused to the *LUC* reporter gene (P1–P5, Supplemental Figure S10B). Activities of the P1, P2, and P3 promoter fragments were similar (Supplemental Figure S10C), implying that P3 contains all the ARF motifs required for *ILA1* activation. Promoter activity decreased significantly for the P4 construct (Supplemental Figure S10C), indicating that the 191-bp region upstream of the *ILA1* start codon, which contained the only Aux RE site, could drive gene transcription, but not as well as the full-length promoter. The P5 construct was not functional in activating *LUC* gene expression (Supplemental Figure S10C).

To confirm these conclusions, we performed chromatin IP-quantitative polymerase chain reaction (ChIP-qPCR) using GFP antibody against GFP-tagged OsARF6 and OsARF17 proteins (Supplemental Figure S5D). Fragments for amplification included CF (present only in P1, with 4 Aux RE-L motifs); CF1 (present in P3, 2 Aux RE-L motifs); and CF2 (present in P4, containing the only Aux RE motif and 2 Aux RE-Ls; Figure 5A). Enrichment was detected in CF1 and CF2 fragments for OsARF6 and OsARF17 independently (Figure 5, C and D), indicating that the two ARF proteins can physically bind to these regions of the *ILA1* promoter in vivo. We performed an electrophoretic mobility shift assay (EMSA) to verify the interaction between OsARF6 and OsARF17 with these regions of the *ILA1* promoter. Two probes (M1 and M2) were designed to bind to an Aux RE-L motif in CF1, and the Aux RE motif in CF2 fragments, respectively (Figure 5A). Our results indicate that OsARF6 and OsARF17 directly interact with the M1 and M2 probes in vitro (Figure 5, E and F). These results demonstrated that regions of the *ILA1* promoter can be bound directly by OsARF6 and OsARF17 in vivo and in vitro to activate downstream gene transcription.

If the expression of *ILA1* is activated by OsARF6 and OsARF17, we would expect reduced *ILA1* transcription in *dm* compared to WT plants when auxin is added. We therefore assessed the expression level of *ILA1* in the WT versus *dm* lamina joints after NAA treatment. RT-qPCR analysis revealed reduced expression level of *ILA1* in *dm* as compared to WT flag leaf lamina joints; furthermore, *ILA1* expression was induced by NAA only in the WT, but not in *dm*, flag leaf lamina joints (Figure 5G). These results demonstrate that auxin regulates *ILA1*-mediated flag leaf angle through OsARF6 and OsARF17.

Our results therefore pointed towards a mechanism where OsARF6 and OsARF17 act upstream of *ILA1* in a common pathway to modulate flag leaf angles. To further verify these findings, we generated transgenic plants overexpressing *ILA* in the *osarf6* background. As expected, the flag leaf angles

of *osarf6* were reduced by the overexpression of *ILA1* in a dose-dependent manner (Figure 5, H–J). These results demonstrated that *ILA1* is an important downstream component of auxin-mediated secondary cell wall biosynthesis signaling.

OsARF6 and OsARF17 maintain grain yield in densely planted rice

Flag leaf angle is a key breeding trait determining grain yield, as it affects how densely crops can be planted (Tian et al., 2019). It may thus be expected that *dm* plants produce less grain compared to the WT when densely planted. To test this hypothesis, we planted WT and *dm* lines at three different planting densities. At low planting densities, we did not detect any obvious differences in grain yield per panicle in WT and *dm* plants (Figure 6, A and B). Furthermore, primary tillers per plant and spikelet number per panicle were not changed in *dm* compared to the WT at different planting densities (Figure 6, C and D). In contrast, both medium and high planting densities resulted in reduced grain yield (Figure 6, A and B), likely resulting from increased percentage of empty grain per panicle in *dm* as compared to WT plants (Figure 6, A and E). These results indicate that OsARF6 and OsARF17 are important to sustain grain yield under dense planting conditions.

Discussion

The flag leaf angle represents a major component of plant architecture of interest to plant breeders as it affects yield by influencing agronomic traits such as planting density (Tian et al., 2019). Crops with more erect flag leaves have been a breeding target for several decades (Peng et al., 1994, 1999). However, the mechanistic basis of flag leaf angle regulation is not yet well understood.

Here, we report that mutants disrupting two components of the auxin-response pathway, OsARF6 and OsARF17, exhibit large flag leaf angles (Figure 1, D–F andFigure 2, O and P), consistent with the observation that reduction in free auxin by the overexpression of auxin-conjugating enzymes caused a larger flag leaf angle in transgenic plants (Zhang et al., 2009; Du et al., 2012; Zhao et al., 2013). Both *OsARF6* and *OsARF17* are expressed in flag leaf lamina joints, and the encoded proteins work together to regulate the secondary cell wall biosynthesis of Sc in the lamina joints (Figures 3 and 4; Supplemental Movies S3 and S4). OsARF12, OsARF17, and OsARF25 regulate tiller angle (Li et al., 2020). The leaf and tiller angles were not affected in our *dm* (Supplementary Figure S4, A–E), likely due to genetic redundancy in these tissues with other *OsARFs*, such as *OsARF12* and *OsARF25*. This hypothesis is further supported by the expression patterns of the genes (Supplementary Figure S5A).

OsARF6 and OsARF17 regulate flag leaf angle by directly activating the expression of *ILA1* (Figure 5, A–F; Supplemental Figure S10). *ILA1* controls the secondary cell wall biosynthesis of internodes and its loss-of-function mutants exhibit decreased lignin and cellulose content (Zhang et al., 2018), similar to what we found in the *dm* lamina joints (Supplemental Figure S6). As a MAPKKK (Ning et al., 2011), ILA1 likely phosphorylates several downstream components, such as IIP4, which, when activated, moves to the cytoplasm to lift the repression of NACs-MYB61 that regulate the secondary cell wall biosynthesis (Zhang et al., 2018). We show that auxin induces the expression of *ILA1* via OsARF6 and OsARF17 in the lamina joint of flag leaf (Figure 5G), providing a mechanistic link between auxin signaling and secondary cell wall biosynthesis pathways.

Our study outlines how auxin-induced secondary cell wall biosynthesis of sclerenchymatous tissues affects the mechanical strength of the lamina joints that allows WT joints to support the weight of the flag leaf throughout its development, while the weaker *dm* joints cannot sustain an erect flag leaf blade (Figure 3; Supplemental Figure S7). This defect is different from that of the altered flag leaf angle in BR signaling mutants, which is due to the modified cell expansion and propagation of collar adaxial cells and the cell proliferation of abaxial cells (Bai et al., 2007; Sun et al., 2015). As *ila1* mutants exhibited a similar BR response to WT lines (Ning et al., 2011), auxin and BR signals appear to play distinct roles in leaf angle regulation. As auxin–BR interactions are known to coordinate other elements of plant growth, such as lateral root growth, shade avoidance, and hypocotyl elongation (Kozuka et al., 2010; Cho et al., 2014; Liu et al., 2018), it will be interesting to untangle their respective contributions during leaf angle maintenance.

In summary, we demonstrate that two auxin-regulated transcription factors, OsARF6 and OsARF17, modulate flag leaf angle by reinforcing mechanical tissues to ensure flag leaf erectness and high grain yield of densely planted rice. Moreover, our work identifies a regulatory mechanism by which OsARF6 and OsARF17 directly activate *ILA1* expression to modulate flag leaf angle (Figure 6F). Our study provides new avenues of flag leaf angle adjustment by fine-tuning secondary cell wall biosynthesis in lamina joints to breed new crop lines with erect flag leaves.

Materials and methods

Plant materials and growth conditions

The background of all rice plants in this study was *Oryza sativa* L. ssp. *japonica* cv. ZH11. Rice materials were grown in a paddy field at Shanghai (30°N, 121°E) in the summer and Sanya (18°N, 109°E) in the winter. The T-DNA insertion lines *osarf6* (RMD_04Z11MS49) and *osarf17* (RMD_03Z11BY76) were obtained from Rice Mutant Database (http://rmd.ncpgr.cn/). The single or double mutants of *OsARF6* and *OsARF17* were analyzed by genotyping PCR (Supplemental Table 1). Planting densities for yield trials were 49 plants/m^2 (high), 36 plants/m^2 (medium), and 25 plants/m^2 (low). The CRISPR/Cas9 mutants for OsARF6 and OsARF17 were generated by EDGENE BIOT company (http://www.edgene.com.cn/).

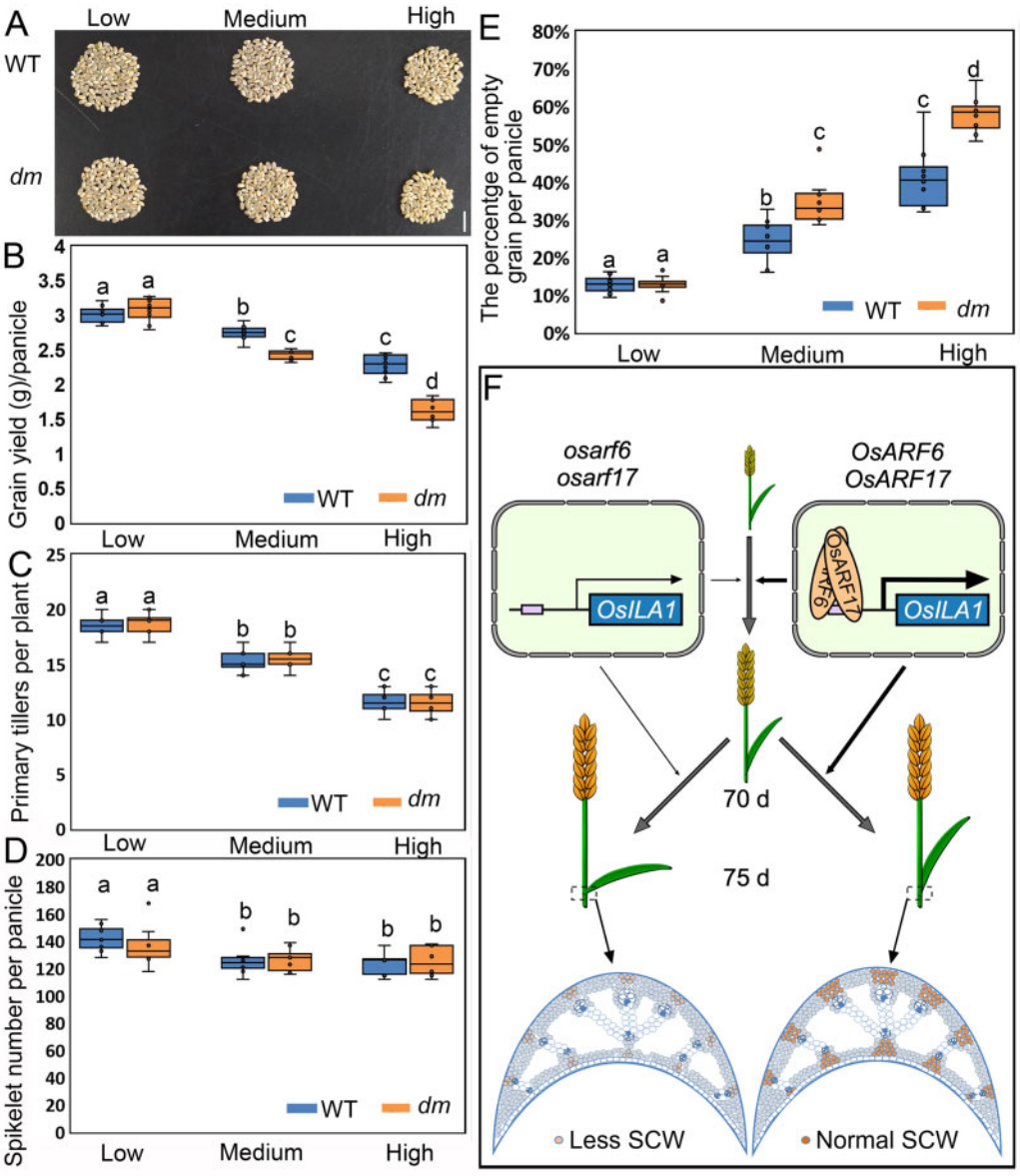

Figure 6 The grain yield of *dm* was decreased under dense planting conditions. A, Uncoated seeds from one WT or *dm* panicle grown in high (49 plants/m^2), medium (36 plants/m^2), and low planting (25 plants/m^2) densities. Bar, 1 cm. B, Grain yield per WT or *dm* panicle at high, medium, and low planting densities. Boxplots show the distribution of grain yield per panicle in WT and *dm* lines. The horizontal bar within box represents the median. The top and bottom of the box represent the 0.75 and 0.25 percentiles, respectively. The upper and lower whiskers extend to 1.5 times the interquartile range, with outliers shown as black dots. Different characters indicate significant differences (Student's *t* test, $P < 0.01$). C, Primary tiller number per WT or *dm* plant at high, medium, and low planting densities. Boxplots show the distribution of primary tiller number per plant in WT and *dm* lines. The horizontal bar within box represents the median. The top and bottom of the box represent the 0.75 and 0.25 percentiles, respectively. The upper and lower whiskers extend to 1.5 times the interquartile range, with outliers shown as black dots. Different characters indicate significant differences (Student's *t* test, $P < 0.01$). D, Spikelet number per WT or *dm* panicle at high, medium, and low planting densities. Boxplots show the distribution of spikelet number per plant in WT and *dm* lines. The horizontal bar within box represents the median. The top and bottom of the box represent the 0.75 and 0.25 percentiles, respectively. The upper and lower whiskers extend to 1.5 times the interquartile range, with outliers shown as black dots. Different characters indicate significant differences (Student's *t* test, $P < 0.01$). E, Percentage of empty grain per WT or *dm* panicle at high, medium, and low planting densities. Boxplots show the distribution of percentage of empty grain per panicle in WT and *dm* lines. The horizontal bar within box represents the median. The top and bottom of the box represent the 0.75 and 0.25 percentiles, respectively. The upper and lower whiskers extend to 1.5 times the interquartile range, with outliers shown as black dots. Different characters indicate significant differences (Student's *t* test, $P < 0.01$). F, A proposed model for how OsARF6 and OsARF17 maintain mechanical strength of the lamina joints. During development of flag leaf lamina joint, OsARF6 and OsARF17 may form heterodimers and directly activate the expression of *ILA1*, which is required for the normal Sc development that provides the mechanical strength to support erect flag leaves. Deficiency of *OsARF6* and *OsARF17* causes reduced expression of *ILA1* and leads to larger flag leaf angle ascribed to impaired mechanical strength of the tissue. MicroCT imaging the abaxial region of flag leaf lamina joint at maturity stage in rice. Secondary cell wall was thickened around the vascular bundle. This tissue provides strength for maintaining flag leaf erectness. Bar, 20 μm.

NAA treatment

A total of 100 mL of 0.5% (w/v) agar was prepared and cooled to 40°C before adding 10-μL 1-mM NAA or water. Once set, agar was sliced into strips and kept at 4°C. Strips (with or without NAA) were carefully placed on the lamina joints of flag leaves at 17:00 to avoid damage, and replaced every day for 10 days. To generate tissues for RT-qPCR analysis, the sliced agar with or without NAA was carefully placed on the lamina joints of flag leaves at 17:00 and the flag leaf lamina joints were collected after a 2-h treatment.

RT-PCR, RT-qPCR, and plasmid construction

Total RNA was extracted from the flag leaf lamina joints after 60 days of growth using TRIzol reagent (Invitrogen) according to the manufacturer's instructions. Reverse transcription was performed using a Reverse Tra Ace-a-First strand cDNA synthesis kit (TOYOBO). RT-PCR was performed using Taq Master Mix (Vazyme) with primers for *OsARF6*, *OsARF17*, and *Actin* (Supplemental Table 1). QRT-PCR was performed using a SYBR Green PCR kit (Qiagen) with primers for *OsARF6*, *OsARF12*, *OsARF17*, *OsARF25*, *ILA1*, *UBQ*, and *TUB* (Supplemental Table 1), where *TUB* and *UBQ* genes were used as internal controls. All cloned PCR amplifications were done with KOD One PCR Master Mix (TOYOBO) with the suggested annealing temperature (37°C) and extension time (15 min) according to fragment length (Supplemental Table S1). Sequences were analyzed and aligned by SnapGene (https://www.snapgene.com/). PCR products and vectors were purified with a QIAquick Spin miniprep kit (Qiagen). The expression vectors were constructed by In-fusion technology (https://www.takarabio.com/). For each construct, more than 15 independent transgenic plants were obtained. *pCAMBIA1301-GFP* was used as the binary vector for tagging *OsARF6* or *OsARF17* clones with GFP; *pCAMBIA1301-GUS* was used as the binary vector for expressing GUS under the control of *OsARF* promoters.

GUS staining procedure and cell wall labeling

The methods for GUS staining of *ProOsARF6/17:GUS* were modified from a previously published protocol (Kong et al., 2019). Briefly, lamina joints of flag leaf at different stages were incubated in GUS staining solution (50-mM $NaPO_4$ buffer, pH 7.0, 10-mg mL^{-1} X-Gluc, and 0.02% (v/v) Triton X-100), at 37°C in the dark for 12 h, and then washed with 70% (v/v) ethanol for 72 h twice until transparent. The GUS staining images were captured via a Leica light microscope (M205A) with a CCD camera. The sections of GUS-stained samples were sliced by microtome (Leica VT 1000s), and photographed using a light microscope (H600L, Nikon).

For lignin staining with phloroglucinol–HCl, hand-cut sections of lamina joints were incubated in HCl acid for 3 min, and then stained with 5% (w/v) phloroglucinol–HCl 5% (w/v) solution composed of phloroglucinol (Sigma) dissolved in 95% (v/v) ethanol. All sections were imaged using a light microscope coupled to a CCD camera (H600L, Nikon) with representative images shown.

For cellulose staining, 5-μm sections of paraffin-embedded samples were cut using a wax microtome and collected on a glass slide. After dewaxing and drying, sections were immunolabeled using the HIS-tagged carbohydrate binding module 3a (CBM3a) probe (Plant Probes) at 1:50 dilution in a blocking buffer of 1% (w/v) bovine serum albumin in phosphate buffered saline (PBS) overnight at 4°C. Sections were washed in PBS three times for 5 min each, and incubated with 1:100 dilution anti-HIS tag antibody (H1029, Sigma) in blocking buffer for 2 h at room temperature. The sections were again washed three times in PBS and then incubated in a 1:200 dilution of the secondary antibody Alexa Fluor 568 (A11031, Life Technologies) in blocking buffer for a further 2 h. Sections were rinsed again with PBS and imaged using a Nikon C2 confocal microscope using the 561 nm laser line and collecting the emission spectrum from 580–649 nm. The settings for all samples were identical.

Lignin and cellulose content measurements

For lignin content measurement, samples were ground in liquid nitrogen. Samples were washed twice with 95% (v/v) ethanol, centrifuged at 700*g*, 25°C for 2 min, and dried in an oven at 30°C until a constant weight was achieved. Dry samples (20 mg) were placed into screwcap centrifuge tubes containing 2-mL 25% (v/v) acetyl bromide in glacial acetic acid and incubated at 70°C for 30 min. After complete digestion, 0.2 mL of sample was mixed with 0.45-mL 2 M NaOH, 0.05 mL of 7.5 M hydroxylamine–HCl, and 3.3 mL of glacial acetic acid. The mixed solution was diluted to 10 mL with glacial acetic acid. The absorbance of the supernatant was measured at 280 nm, and absorbance results converted to lignin amounts as previously described (Zhang et al., 2018). Cellulose measurements were performed as described by Zhang et al. (2018).

Y2H/Y1H assays and EMSA

For Y1H assays, full-length CDS of *OsARF6/17* and the promoter of *ILA1* were amplified (primers in Supplemental Table S1) and independently cloned into the yeast one-hybrid vector, pHIS2 (Clontech). Y1H experiments were performed using the Matchmaker Gold Yeast One-Hybrid System kit (Clontech). Confirmation of OsARF6 or OsARF17 interaction with the *ILA1* promoter was conducted in SD/-Trp/-Leu/-His medium containing 0 and 80-mM 3-amino-1, 2, 4-triazole (3-AT).

For Y2H assays, full-length cDNAs of *OsARF6* and *OsARF17* were amplified (primers in Supplemental Table S1) and cloned into Y2H vectors, pGBKT7 and pGADT7 (Clontech), respectively. Y2H experiments were performed according to instructions for the Matchmaker Gold Yeast Two-Hybrid System (Clontech). Detection of OsARF6-OsARF17 interactions were verified in SD/-Trp/-Leu/-His medium containing 40-mM 3-AT.

For EMSAs, OsARF6 and OsARF17 were synthesized using the Single-Tube Coupled Transcription/Translation System (Promega) using 2 μg BD-HA-OsARF6 and AD-HA-OsARF17 vectors. The synthesized proteins were verified by HA tag.

Double-stranded M1 and M2 oligonucleotide probes were synthesized with forward/reverse primers with and without 5′-end modification with 6-carboxyfluorescein (6-FAM) dye (Supplemental Table S1). The competitors were the double-stranded oligonucleotide without any modification. The probe-annealing EMSA reactions were performed in a total volume of 10 μL of binding buffer (20-mM HEPES-KOH, pH 7.9, 100-mM KCl, 2-mM DTT, and 20% glycerol) containing 2-μL OsARF6/17 synthesized solution, and either 80-ng M1 or M2 labeled probe (×1), or 64-ng M1 or M2 nonlabeled probe and 16-ng M1 or M2 labeled probe (×5). EMSA reaction products were resolved on a 6% polyacrylamide gel. The results were captured through Cy2 filters: excitation (460 nm) laser and 510–550 nm emission installed in a GE Amersham Imager 680.

BiFC, Co-IP, and ChIP–PCR assays

The BiFC and Co-IP experiments were performed in the leaves of *N. benthamiana* plants. Plants were grown under a 16-h-light/8-h-dark cycle at 22°C for 21 days. Suspensions of *Agrobacterium tumefaciens* GV3101 transformed with appropriate vectors were adjusted to optical density at 600 nm (OD_{600}) = 0.8 in MES medium (50-mM $MgCl_2$, 50-mM MES, and 200-μM acetosyringone, pH 5.7), prior to infiltrating the fifth and sixth leaves of plants. After infiltration, plants were kept in the glasshouse for 48 h before analysis.

BiFC procedures were performed as described previously (Huang et al., 2013). After *OsARF6* and *OsARF17* cDNAs were individually cloned (primers in Supplemental Table S1) into pXY104 and pXY106, containing either the C- or N-terminal domain of enhanced yellow fluorescent protein (Mao et al., 2020), respectively. The vector was transformed into *Agrobacterium* and transiently expressed in *N. benthamiana* leaves for 48 h. The results were captured through YFP filters: excitation (514 nm) laser and 525–550 nm emission installed in Leica SP5.

Co-IP assays were performed with leaves of 18-day *N. benthamiana* plants. *OsARF6 OsARF17* cDNAs were individually cloned into pGreen-FLAG and pGreen-HA vectors and transiently expressed in *N. benthamiana* leaves for 48 h after *Agrobacterium*-mediated transformation. Infiltrated leaves of 0.5 g were harvested and ground in liquid nitrogen. Leaf powder was mixed with 1-mL extraction buffer (20-mM HEPES-KOH at pH 7.5, 40-mM KCl, 1-mM EDTA, 0.5% (V/V) Triton X-100, and 1-mM PMSF). After centrifugation for 10 min at 16,200*g*, the supernatant was incubated with 50-μL prepared protein G-agarose (7033823, Roche) for 1 h with gentle rotation at 4°C to clear the background. After centrifugation for 3 min at 500*g*, the supernatant was incubated with anti-FLAG (1:300, mouse, 314570, Abmart) or anti-HA (1:300, mouse, 304585, Abmart) antibodies for 12 h with gentle rotation at 4 °C. Fifty microliters of prepared protein G-agarose was added into the incubated mix and maintained for 1 h at 4°C with gentle rotation. Then, the mix was centrifuged at 4°C, 500*g* for 3 min to collect the pellet. The collected pellet was washed with 200-μL extraction buffer five times, each with gentle rotation for 5 min at 4°C and pelleted at 500*g* for 3 min. Finally, the pellets were resuspended in 100-μL extraction buffer and 100-μL SDS buffer (250-mM Tris–HCl [pH 6.8], 10% SDS [w/v], 0.5% bromophenol blue [w/v], 50% glycerol [v/v]), and heated at 95°C for 5 min. The samples were centrifuged at 500*g* at 25 °C for 3 min and the supernatants were analyzed by immunoblot analysis, for which primary antibodies (anti-HA, 314570, Abmart and anti-FLAG, 304585, Abmart) were diluted 1:5,000, and the secondary goat anti-mouse polyclonal antibody (ab6789, Abmart) conjugated with horseradish peroxidase (HRP) was diluted 1:20,000. HRP staining was according to manufacturer's instructions (SuperSignal West Atto, ThermoFisher). The images were captured by GE ImageQuant LAS4000mini.

ChIP–PCR procedures were conducted according to a reported protocol (Haring et al., 2007). Flag leaf lamina joints (65 days after planting) were harvested and cross-linked in 1% (w/v) formaldehyde under vacuum for 50 min, quenched by 0.25 M glycine for 5 min, washed in ddH_2O five times, and ground in liquid nitrogen. Nuclei were precipitated by centrifugation at 3,000*g* and sheared into ∼100- to 300-bp fragments by sonication; nonsonicated chromatin DNA was reverse cross-linked and used as the total input DNA control. IP was performed using an anti-GFP antibodies (rabbit monoclonal, ab32146, Abcam) bound to Protein G agarose/salmon sperm DNA (16-201, Sigma). The IP proteins and DNA were eluted with 1% (w/v) SDS and 0.1 M $NaHCO_3$, and the cross-linking was reversed by incubation in 250-mM NaCl at 65°C for 12 h. qPCR was performed on IP genomic DNA, and the relative enrichment was normalized to input for each sample (primers in Supplemental Table S1).

Luciferase assays

The dual-LUC method was performed in the *N. benthamiana* leaves. *Pro35S:FLAG-ARF6* and *Pro35S:HA-ARF17* were used as effector constructs. The reporter constructs *ProP1:LUC*, *ProP2:LUC*, *ProP3:LUC*, *ProP4:LUC*, and *ProP5:LUC* were constructed based on pGreenII-0800-LUC. Effector and reporter plasmids were transiently expressed in *N. benthamiana* leaves for 48 h after Agrobacterium-mediated transformation as described above. 1 cm^2 infiltrated leaves were harvested and ground in liquid nitrogen. LUC and REN activities were measured using the dual-LUC assay reagent kit (Promega) with the GLOMAX 20/20 luminometer (Promega), according to the manufacturer's instructions. Promoter activities were evaluated by normalizing LUC activities to REN activities.

CT scanning

For CT scanning procedures, the lamina joints of flag leaves were fixed in FAA (60% (v/v) ethanol, 6% (v/v) acetic acid, and 5% (v/v) formaldehyde) for 12 h, dehydrated in an ethanol series (70%, 80%, 90%, and 100% v/v), each for 15 min, and then rapidly subjected to final critical point drying. Samples were scanned using an X-ray microscope (CT, Xradia 520 Versa, Zeiss).

Yield evaluation under different planting densities

Paddy trials were performed in Shanghai 2020. For WT and *dm* lines, each rice plant was grown in a paddy field at a distance of 21.4 × 21.4 cm (25 plants/m^2), 17.6 × 17.7 cm (36 plants/m^2), or 15 × 15 cm (47 plants/m^2). Each treatment was performed in three individual pots with randomized blocks and the size of each pot was 3 × 3 m. Forty plants were harvested and used for analysis from each pot excluding marginal plants. After harvest, the samples were dried for 15 days at 37°C prior to measurements.

Statistical analysis

Two-tailed Student's *t* tests were performed via Microsoft Excel 2020 to detect the statistical significance of data. Statistical data are provided in Supplemental File S1.

Accession numbers

Sequence from this study can be downloaded from the rice genome annotation project (http://rice.plantbiology.msu.edu/) with the following accession numbers: Os*ARF6* Os02g06910; *OsARF12* Os04g57610; *OsARF17* Os06g46410; *OsARF25* Os12g41950; *ILA1* Os06g50920.

Supplemental data

The following materials are available in the online version of this article.

Supplemental Figure S1. Characterization of *osarf6* and *osarf17* T-DNA insertion mutants.

Supplemental Figure S2. *OsARF6* and *OsARF17* are expressed in both abaxial and adaxial regions.

Supplemental Figure S3. Knockout mutants of *OsARF6* and *OsARF17* exhibit a large flag leaf angle.

Supplemental Figure S4. The height, leaf angle, and tiller angle are normal in *dm*.

Supplemental Figure S5. The expression pattern of *OsARFs* in rice tissues.

Supplemental Figure S6. Lignin and cellulose contents were reduced in *dm* lamina joints but not stems.

Supplemental Figure S7. Fresh weight analysis of WT and *dm* flag leaves from 60 to 90 days after planting.

Supplemental Figure S8. Lignin and cellulose contents were reduced in *ila1* lamina joints but not stems.

Supplemental Figure S9. Secondary cell wall structure was defective in lamina joints of *ila1* flag leaves.

Supplemental Figure S10. Characterization of a series of *ProILA1:LUC* constructs in *N. benthamiana* leaves.

Supplemental Table S1. Primers used in this work.

Supplemental Movie S1. Phenotypic analysis of the WT lamina joint of flag leaf using CT scanning.

Supplemental Movie S2. Phenotypic analysis of *dm* lamina joint of flag leaf using CT scanning.

Supplemental Movie S3. Sections of the WT lamina joint from top to down via CT scanning images.

Supplemental Movie S4. Sections of *dm* lamina joint from top to down via CT scanning images.

Supplemental Movie Legends.

Supplemental File S1. Summary of statistical tests.

Acknowledgments

We thank Prof. Lizhong Xiong and Yihua Zhou for providing *ila1* seeds; MingJiao Chen and Xiaofei Chen for rice transformation; and Zhijing Luo for rice cultivation.

Funding

This work was supported by the National Key Research and Development Program of China (2016YFD0100804 and 2016YFD0100903), the National Natural Science Foundation of China (31861163002 and 31700276), the Innovative Research Team, Ministry of Education, and 111 Project (B14016), the China Postdoctoral Science Foundation (2019M661486), the fellowship of China Postdoctoral Science Foundation (2021T140446), and Shanghai Post-doctoral Excellent Program (2018063). S.P. acknowledges the Australian Research Council (DP190101941), Villum Investigator (Project ID: 25915), DNRF Chair award (DNRF155), and Novo Nordisk Laureate (NNF19OC0056076) grants.

Conflict of interest statement. The authors declare no conflict of interest.

References

Bai M-Y, Zhang L-Y, Gampala SS, Zhu S-W, Song W-Y, Chong K, Wang Z-Y (2007) Functions of OsBZR1 and 14-3-3 proteins in brassinosteroid signaling in rice. Proc Natl Acad Sci U S A **104**: 13839–13844

Cao H, Chen S (1995) Brassinosteroid-induced rice lamina joint inclination and its relation to indole-3-acetic acid and ethylene. Plant Growth Regul **16**: 189–196

Chen Y, Dan Z, Gao F, Chen P, Fan F, Li S (2020) *Rice GROWTH-REGULATING FACTOR7* modulates plant architecture through regulating GA and indole-3-acetic acid metabolism. Plant Physiol **184**: 393–406

Chen Y, Yuan L-P, Wang X-H, Zhang D-Y, Chen J, Deng Q-Y, Zhao B-R, Xu D-Q (2007) Relationship between grain yield and leaf photosynthetic rate in super hybrid rice. Zhi Wu Sheng Li Yu Fen Zi Sheng Wu Xue Xue Bao **33**: 235

Cho H, Ryu H, Rho S, Hill K, Smith S, Audenaert D, Park J, Han S, Beeckman T, Bennett MJ, et al. (2014). A secreted peptide acts on BIN2-mediated phosphorylation of ARFs to potentiate auxin response during lateral root development. Nat Cell Biol **16**: 66–76

Dong HJ, Zhao H, Li SL, Han ZM, Hu G, Liu C, Yang GY, Wang GW, Xie WB, Xing YZ (2018) Genome-wide association studies reveal that members of bHLH subfamily 16 share a conserved function in regulating flag leaf angle in rice (*Oryza sativa*). PloS Genet **14**: e1007323

Du H, Wu N, Fu J, Wang S, Li X, Xiao J, Xiong L (2012) A GH3 family member, OsGH3-2, modulates auxin and abscisic acid levels and differentially affects drought and cold tolerance in rice. J Exp Bot **63**: 6467–6480

Freire-Rios A, Tanaka K, Crespo I, van der Wijk E, Sizentsova Y, Levitsky V, Lindhoud S, Fontana M, Hohlbein J, Boer DR, et al. (2020). Architecture of DNA elements mediating ARF transcription factor binding and auxin-responsive gene expression in *Arabidopsis*. Proc Natl Acad Sci USA **117**: 24557–24566

Haring M, Offermann S, Danker T, Horst I, Peterhansel C, Stam M (2007) Chromatin immunoprecipitation: optimization, quantitative analysis and data normalization. Plant Methods **3**: 11

Hong Z, Ueguchi-Tanaka M, Shimizu-Sato S, Inukai Y, Fujioka S, Shimada Y, Takatsuto S, Agetsuma M, Yoshida S,

Watanabe Y (2002) Loss-of-function of a rice brassinosteroid biosynthetic enzyme, C-6 oxidase, prevents the organized arrangement and polar elongation of cells in the leaves and stem. Plant J **32**: 495–508

Hong Z, Ueguchi-Tanaka M, Umemura K, Uozu S, Fujioka S, Takatsuto S, Yoshida S, Ashikari M, Kitano H, Matsuoka M (2003) A rice brassinosteroid-deficient mutant, *ebisu dwarf* (*d2*), is caused by a loss of function of a new member of cytochrome P450. Plant Cell **15**: 2900–2910

Huang GQ, Li E, Ge FR, Li S, Wang Q, Zhang CQ, Zhang Y (2013) Arabidopsis RopGEF4 and RopGEF10 are important for FERONIA-mediated developmental but not environmental regulation of root hair growth. New Phytol **200**: 1089–1101

Jiao Y, Wang Y, Xue D, Wang J, Yan M, Liu G, Dong G, Zeng D, Lu Z, Zhu X (2010) Regulation of *OsSPL14* by OsmiR156 defines ideal plant architecture in rice. Nat Genet **42**: 541

Kang X, Kirui A, Dickwella Widanage MC, Mentink-Vigier F, Cosgrove DJ, Wang T (2019) Lignin-polysaccharide interactions in plant secondary cell walls revealed by solid-state NMR. Nat Commun **10**: 347

Kong X, Huang G, Xiong Y, Zhao C, Wang J, Song X, Giri J, Zuo K (2019) IBR5 regulates leaf serrations development via modulation of the expression of *PIN1*. Int J Mol Sci **20**: 429

Kozuka T, Kobayashi J, Horiguchi G, Demura T, Sakakibara H, Tsukaya H, Nagatani A (2010) Involvement of auxin and brassinosteroid in the regulation of petiole elongation under the shade. Plant Physiol **153**: 1608–1618

Li D, Wang L, Wang M, Xu YY, Luo W, Liu YJ, Xu ZH, Li J, Chong K (2009) Engineering *OsBAK1* gene as a molecular tool to improve rice architecture for high yield. Plant Biotechnol J **7**: 791–806

Li H, Jiang L, Youn JH, Sun W, Cheng Z, Jin T, Ma X, Guo X, Wang J, Zhang X (2013) A comprehensive genetic study reveals a crucial role of CYP90D2/D2 in regulating plant architecture in rice (*Oryza sativa*). New Phytol **200**: 1076–1088

Li Y, Li J, Chen Z, Wei Y, Qi Y, Wu C (2020) OsmiR167a-targeted auxin response factors modulate tiller angle via fine-tuning auxin distribution in rice. Plant Biotechnol J **18**: 2015–2026

Liu K, Li Y, Chen X, Li L, Liu K, Zhao H, Wang Y, Han S (2018) ERF72 interacts with ARF6 and BZR1 to regulate hypocotyl elongation in *Arabidopsis*. J Exp Bot **69**: 3933–3947

Mairhofer S, Zappala S, Tracy S, Sturrock C, Bennett MJ, Mooney SJ, Pridmore TP (2013) Recovering complete plant root system architectures from soil via X-ray μ-computed tomography. Plant Methods **9**: 8

Mao Z, He S, Xu F, Wei X, Jiang L, Liu Y, Wang W, Li T, Xu P, Du S, et al. (2020). Photoexcited CRY1 and phyB interact directly with ARF6 and ARF8 to regulate their DNA-binding activity and auxin-induced hypocotyl elongation in *Arabidopsis*. New Phytol **225**: 848–865

Moldenhauer KA, Gibbons JH, Smith C, Dilday R (2003) Rice Morphology and Development. John Wiley & Sons, Inc., Hoboken, NJ

Ning J, Zhang B, Wang N, Zhou Y, Xiong L (2011) Increased leaf angle1, a Raf-like MAPKKK that interacts with a nuclear protein family, regulates mechanical tissue formation in the lamina joint of rice. Plant Cell **23**: 4334–4347

Peng S, Khush G, Cassman K (1994) Evolution of the new plant ideotype for increased yield potential. In K Cassman, ed, Breaking the Yield Barrier, Vol 5. International Rice Research Institute, Los Baños, Philippines, p 20

Peng S, Cassman KG, Virmani S, Sheehy J, Khush G (1999) Yield potential trends of tropical rice since the release of IR8 and the challenge of increasing rice yield potential. Crop Sci **39**: 1552–1559

Sakamoto T, Morinaka Y, Ohnishi T, Sunohara H, Fujioka S, Ueguchi-Tanaka M, Mizutani M, Sakata K, Takatsuto S, Yoshida S (2006) Erect leaves caused by brassinosteroid deficiency increase biomass production and grain yield in rice. Nat Biotechnol **24**: 105–109

Shen C, Wang S, Bai Y, Wu Y, Zhang S, Chen M, Guilfoyle TJ, Wu P, Qi Y (2010) Functional analysis of the structural domain of ARF proteins in rice (*Oryza sativa* L.). J Exp Bot **61**: 3971–3981

Shimada A, Ueguchi-Tanaka M, Sakamoto T, Fujioka S, Takatsuto S, Yoshida S, Sazuka T, Ashikari M, Matsuoka M (2006) The rice SPINDLY gene functions as a negative regulator of gibberellin signaling by controlling the suppressive function of the DELLA protein, SLR1, and modulating brassinosteroid synthesis. Plant J **48**: 390–402

Sun S, Chen D, Li X, Qiao S, Shi C, Li C, Shen H, Wang X (2015) Brassinosteroid signaling regulates leaf erectness in Oryza sativa via the control of a specific U-type cyclin and cell proliferation. Dev Cell **34**: 220–228

Tian J, Wang C, Xia J, Wu L, Xu G, Wu W, Li D, Qin W, Han X, Chen Q (2019) Teosinte ligule allele narrows plant architecture and enhances high-density maize yields. Science **365**: 658–664

Tong H, Xiao Y, Liu D, Gao S, Liu L, Yin Y, Jin Y, Qian Q, Chu C (2014) Brassinosteroid regulates cell elongation by modulating gibberellin metabolism in rice. Plant Cell **26**: 4376–4393

Ueguchi-Tanaka M, Fujisawa Y, Kobayashi M, Ashikari M, Iwasaki Y, Kitano H, Matsuoka M (2000) Rice dwarf mutant *d1*, which is defective in the alpha subunit of the heterotrimeric G protein, affects gibberellin signal transduction. Proc Natl Acad Sci USA **97**: 11638–11643

Wang R, Liu C, Li Q, Chen Z, Sun S, Wang X (2020) Spatiotemporal resolved leaf angle establishment improves rice grain yield via controlling population density. iScience **23**: 101489

Wu C, Li X, Yuan W, Chen G, Kilian A, Li J, Xu C, Li X, Zhou DX, Wang S (2003) Development of enhancer trap lines for functional analysis of the rice genome. Plant J **35**: 418–427

Yamamuro C, Ihara Y, Wu X, Noguchi T, Fujioka S, Takatsuto S, Ashikari M, Kitano H, Matsuoka M (2000) Loss of function of a rice brassinosteroid insensitive1 homolog prevents internode elongation and bending of the lamina joint. Plant Cell **12**: 1591–1605

Zhang D, Xu Z, Cao S, Chen K, Li S, Liu X, Gao C, Zhang B, Zhou Y (2018) An uncanonical CCCH-tandem zinc-finger protein represses secondary wall synthesis and controls mechanical strength in rice. Mol Plant **11**: 163–174

Zhang H, Zhang J, Wei P, Zhang B, Gou F, Feng Z, Mao Y, Yang L, Zhang H, Xu N (2014) The CRISPR/Cas9 system produces specific and homozygous targeted gene editing in rice in one generation. Plant Biotechnol J **12**: 797–807

Zhang J, Li C, Wu C, Xiong L, Chen G, Zhang Q, Wang S (2006) RMD: a rice mutant database for functional analysis of the rice genome. Nucleic Acids Res **34**: D745–D748

Zhang S-W, Li C-H, Cao J, Zhang Y-C, Zhang S-Q, Xia Y-F, Sun D-Y, Sun Y (2009) Altered architecture and enhanced drought tolerance in rice via the down-regulation of indole-3-acetic acid by *TLD1/OsGH3.13* activation. Plant Physiol **151**: 1889–1901

Zhang S, Wang S, Xu Y, Yu C, Shen C, Qian Q, Geisler M, Jiang DA, Qi Y (2015) The auxin response factor, OsARF 19, controls rice leaf angles through positively regulating OsGH3-5 and OsBRI1. Plant Cell Environ **38**: 638–654

Zhao S-Q, Xiang J-J, Xue H-W (2013) Studies on the rice LEAF INCLINATION1 (LC1), an IAA–amido synthetase, reveal the effects of auxin in leaf inclination control. Mol Plant **6**: 174–187

Zhou L-J, Xiao L-T, Xue H-W (2017) Dynamic cytology and transcriptional regulation of rice lamina joint development. Plant Physiol **174**: 1728–1746